



OPEN ACCESS

EDITED BY Arif Nur Muhammad Ansori, Universitas Airlangga, Indonesia

REVIEWED BY
Harapan Harapan,
Syiah Kuala University, Indonesia
Supasek Kongsomros,
University of Cincinnati, United States
Aham Emmanuel Chigozie,
University of Nigeria Enugu Nigeria, Nigeria

*CORRESPONDENCE
Si-Whan Song
Swansong@csco.co.kr
Jong-Choon Kim
toxkim@jnu.ac.kr

RECEIVED 13 August 2025 ACCEPTED 28 October 2025 PUBLISHED 17 November 2025

CITATION

An J-S, Kim W-I, Hong S-T, Kim H-M, Kwon O-Y, Lee J-H, Kim YC, Lee M-H, Kim J-C and Song S-W (2025) Oral administration of Korean perilla frutescens leaf extract shows potential therapeutic effects against COVID-19 in a SH101 hamster model. *Front. Virol.* 5:1685444. doi: 10.3389/fviro.2025.1685444

COPYRIGHT

© 2025 An, Kim, Hong, Kim, Kwon, Lee, Kim, Lee, Kim and Song. This is an open-access article distributed under the terms of the Creative Commons Attribution License (CC BY). The use, distribution or reproduction in other forums is permitted, provided the original author(s) and the copyright owner(s) are credited and that the original publication in this journal is cited, in accordance with accepted academic practice. No use, distribution or reproduction is permitted which does not comply with these terms.

Oral administration of Korean perilla frutescens leaf extract shows potential therapeutic effects against COVID-19 in a SH101 hamster model

Jin-Soo An^{1,2}, Woong-Il Kim¹, Seong-Tshool Hong³, Hae-Mi Kim³, Oh-Young Kwon², Jae-Hyun Lee², Young Chul Kim², Min-Haeng Lee², Jong-Choon Kim^{1*} and Si-Whan Song^{2*}

¹College of Veterinary Medicine, Chonnam National University, Gwangju, Republic of Korea, ²Nonclinical Research Institute, CorestemChemon Inc, Yongin, Republic of Korea, ³Department of Biomedical Sciences and Institute for Medical Science, Jeonbuk National University Medical School, Jeonju, Republic of Korea

Background and objectives: The outbreak of the COVID-19 pandemic has made the development of effective treatments a critical global issue. This study investigated whether Korean perilla (*Perilla frutescens* var. *frutescens*) leaf ethanol extract (P108) showed therapeutic potential against COVID-19 using the SH101 Roborovski hamster model.

Materials and methods: The COVID-19 infection model was established by intranasal administration of SARS-CoV-2 suspension into SH101 Roborovski hamsters. Experimental groups received P108 at dosages of 1,000 and 3,000 mg/kg/day, with additional groups for normal control (no treatment), vehicle control (0 mg/kg/day with vehicle only), and positive control (Paxlovid at 20 mg/kg/day). All substances were administered orally via gavage using a sonde. Treatment effects were assessed by monitoring changes in body temperature, clinical signs, body weight, levels of D-dimer and fibrin degradation products, interleukin concentrations, viral titers, immune cell counts, and lung pathology. Statistical significance was determined for differences with a p-value ≤ 0.05.

Results: Hamsters infected with SARS-CoV-2 exhibited typical COVID-19 disease progression, including marked hypoactivity by 4 days post-inoculation (dpi). Both P108- and Paxlovid-treated groups initially developed fever but subsequently recovered, with body weight restoration comparable to the normal control group. At 5 dpi, high-dose P108 and Paxlovid treatment resulted in reduced viral loads in lung tissues. Notably, high-dose P108 demonstrated cytokine modulation and viral load reduction trends similar to those observed with Paxlovid, as detailed in the Results and Figure Legends. P108 treatment significantly lowered fibrin degradation product levels, IL-6, and TNF- α while increasing IL-10. Histological analysis showed reduced pulmonary inflammation in the P108-treated groups.

Conclusion: The results of this study suggest that P108 may inhibit SARS-CoV-2 replication and reduce systemic inflammatory responses. These findings support the continued development of P108 as a candidate for preventive or early-intervention strategies against COVID-19. However, its efficacy following delayed treatment initiation (e.g., after symptom onset) has not yet been demonstrated and warrants further investigation.

KEYWORDS

COVID-19, protection, Korean perilla ethanol extracts (P108), cytokine, Roborovski hamster

Introduction

Coronaviruses, first identified approximately 60 years ago, gained attention in 2003 when severe acute respiratory syndrome coronavirus (SARS-CoV) was recognized as the cause of a deadly respiratory infection in humans (1). In November 2019, a novel mutated pathogen, SARS-CoV-2, emerged and precipitated the severe global COVID-19 pandemic (1). Although vaccines against COVID-19 were developed by 2021 and booster programs have been implemented worldwide, the pandemic continues unabated due to the emergence of new viral variants (2-4). Current investigational strategies include the repurposing of existing drugs, such as anti-HIV agents and influenza therapeutics. The ongoing circulation of COVID-19 suggests that, despite their substantial benefits, existing vaccines and treatments are not yet fully optimized to address all viral variants and clinical scenarios (5, 6). While several animal models (e.g., K18-hACE2 mice and Syrian hamsters) have been widely used to study SARS-CoV-2 infection and evaluate therapeutics, each incompletely recapitulates human-like systemic features; therefore, model choice should align with specific study objectives (7). The infection in humans is notably characterized by respiratory symptoms, right-side-dominant pneumonia with more severe inflammation in the right lung than the left, as well as fever, chills, and secondary infections that spread to the brain and liver (8, 9). Existing COVID-19 animal models, which primarily exhibit respiratory symptoms and pneumonia, fall fundamentally short of accurately representing the full spectrum of human COVID-19 pathology (10, 11). Although these models have contributed to advancing research on disease pathogenesis, they fail to fully recapitulate systemic features observed in human patients, thereby limiting translational relevance. As a result, prior animal studies have faced challenges in facilitating the development of optimal vaccines and therapeutics (12). Recently, a research team developed the SH101 Roborovskii hamster (Phodopus roborovskii) model, which accurately reproduces human COVID-19 and exhibits typical characteristics such as respiratory symptoms, right-side-dominant pneumonia, fever, chills, and secondary infections (13). The SH101 Roborovski hamster model was developed to more accurately reflect human-like clinical trajectories, thereby providing a more rigorous platform to

evaluate candidate interventions. Based on this rationale, we investigated *Perilla frutescens* var. *frutescens* (Korean perilla), a food –derived botanical with documented antiviral and immunomodulatory properties, as a plausible early–intervention candidate in this model.

Korean perilla is a widely consumed food plant in Korean cuisine and has long been utilized in traditional Korean medicines. It is traditionally prescribed for stomach-tonifying effects, digestive support, detoxifying properties, regulation of qi, and neutralization of toxic substances (14). Perilla leaves possess several functional properties, including antioxidant, anti-allergenic, antidepressant, anti-inflammatory, and anticancer effects (15, 16). Building upon this rationale, we examined a standardized Korean perilla leaf ethanol extract (P108), enriched in rosmarinic acids, as a plausible preventive or early-intervention candidate under a post -exposure prophylaxis-like design. Korean P. frutescens var. frutescens is distinguished from P. frutescens var. acuta or crispa by the morphology of its leaves, seeds and flowers, and its leaves possess a distinctive aroma and are widely consumed as culinary vegetables exclusively in Korean cuisine (17). Recent research highlights the abundance of rosmarinic acid and caffeic acid (18). Rosmarinic acid has been reported to exhibit anti-inflammatory, antioxidant, antiviral, and antibacterial activities, while caffeic acid possesses notable antibacterial and antiviral properties (19, 20). Metabolites such as phytol in perilla leaves enhance immune function by eliminating cancer cells and pathogenic bacteria (21). In addition, Korean perilla leaves have a unique flavor and may raise pain thresholds through agonist activity at transient receptor potential cation channels, subfamily A (22). Recently, Chinese perilla (P. frutescens var. acuta) leaf water extract was reported to block RNA and protein synthesis in SARS-CoV-2 and to significantly reduce virus-induced cytokine release and viral protein/RNA levels (23). However, to date, no study has investigated the therapeutic efficacy of Korean perilla leaf extract against COVID-19 in either human subjects or laboratory animal models.

This study systematically evaluated the therapeutic potential of P108 for the treatment of COVID-19 using the SH101 Roborovski hamster model, which closely recapitulates human disease

pathology. During the in-life phase, clinical parameters—including symptom progression, body temperature, and body weight—were continuously monitored. To determine the efficacy of P108 against SARS-CoV-2 infection, plasma levels of D-dimer and fibrin degradation products (FDP), biomarkers indicative of pulmonary thrombus formation, were quantified. Furthermore, cytokine profiles associated with hyperinflammatory responses were assessed, and histopathological analyses of lung tissues were conducted to evaluate inflammatory severity and tissue damage.

Materials and methods

Study area

The *in vivo* experiments related to SARS-CoV-2 virus (originated Wuhan) infection and drug administration and the *in vitro* assays were performed at the Animal Biosafety Level 3 facility of the Korea Zoonosis Research Institute Science (Iksan, Republic of Korea) from March to September 2023. UPLC analysis was performed at the Nonclinical Research Center of CORESTEMCHEMON Co. Ltd. (Yongin, Republic of Korea) from February to March 2024.

Chemicals and reagents

Rosmarinic acid [≥98%; high-performance liquid chromatography (HPLC)] standard was purchased from Sigma-Aldrich (St. Louis, MO, USA) and HPLC grade methanol (Lot No. NAG214; J.T. Baker, Phillipsburg, NJ, USA), acetonitrile (Lot No. N9B203; J.T. Baker), deionized water (aquaMAXTM Ultra 370; Anyang, Republic of Korea), and analytical formic acid (Lot No. ACQ1176; WACO, Osaka, Japan) were used for ultra-performance liquid chromatography (UPLC). Paxlovid [nirmatrelvir (Lot No. PF-07321332; AOBIOUS Inc., Gloucester, MA, USA) and ritonavir (Lot No. ABT-538; Selleck Chemicals, Houston, TX, USA)] were purchased for positive control items.

Apparatus and chromatographic conditions

The chromatography analysis was performed using a Waters Acquity TM UPLC system (Waters Corporation, Milford, MA, USA) equipped with an ultraviolet detector, binary solvent manager, and autosampler system. The output signal was monitored and processed using Empower 3 software. An ultrasonic instrument was used for sonication during the sample preparation. The method was developed using a Luna Omega C18 (2.1 × 100 mm) 1.6 μm column (Phenomenex Inc., Torrance, CA, USA) with an isocratic mobile phase containing a mixture of 0.1% formic acid methanol and acetonitrile. The mobile phase was filtered through 0.22 μm membrane filters and degassed. The flow rate of the mobile phase was 0.3 mL/min. The column temperature was maintained at 40 °C

and the eluted compounds were monitored at a wavelength of 330 nm. The sample injection volume was 2 μL .

Preparation of standard solution

Standard rosmarinic acid (1 mg) was weighed accurately and transferred separately into a 10 mL volumetric flask, dissolved in methanol, and sonicated for 5 min; a final volume was made up with methanol to produce a 100 μ g/mL stock solution and working solutions were prepared by stepwise dilution of the stock solution with distilled water to prepare 5.0 μ g/mL.

Preparation of P108 and UPLC analysis of the marker metabolite

The leaves of Korean perilla were collected during September and October from Jeolla-do, Republic of Korea at 2023. The leaves were washed and blanched in boiling water and shade-dried at room temperature. The dried leaves were powdered and subjected to extraction with 70% ethanol (v/v) at room temperature and with continuous stirring for 2 days. The sample was obtained by filtering through a 5-6 µm filter, concentrating, freeze-drying, and pulverizing. The analytical method was validated, in accordance with guidelines from the International Conference on Harmonization, for content, specificity, system suitability, lower limit of quantification, stock standard comparison, performance check standard, linearity, accuracy and precision, homogeneity, and stability. The marker compound, rosmarinic acid in 70% ethanol extracts of Korean perilla leaves was quantified using UPLC. The extract was standardized based on the concentration of the rosmarinic acid, which was set at greater than 100 µg/mg. The method validation was conducted to assess for content, specificity, system suitability (SST), lower limit of quantification (LLOQ), stock standard comparison (SSC), performance check standard (PCS), linearity, accuracy, precision, homogeneity, and stability. No endogenous interfering substances that could affect the quantification of the analyte were identified among the diluents and excipients. The analytical system remained suitable throughout the validation period, and the LLOQ, SSC, and PCS parameters met all predefined acceptance criteria. Rosmarinic acid demonstrated linearity within the concentration range of 0.5 - 5 µg/mL. The QC samples met the criteria for accuracy, precision, and homogeneity.

Experimental animals and animal husbandry

Inbred SH101 Roborovski hamsters were employed as the animal model. Female hamsters, known to exhibit heightened sensitivity compared to males, were selected for this study (13). Three-month-old SH101 Roborovski hamsters were raised in the

animal breeding facility at the College of Medicine, Jeonbuk National University, Jeonju, Republic of Korea. Each cage accommodated no more than five hamsters, which were given free access to food and water (D12450B diet, Research Diets Inc., New Brunswick, NJ, USA) for approximately 7 days for acclimation and general health observation before healthy animals were selected for the efficacy test. The laboratory environment was maintained at $22 \pm 1^{\circ}\text{C}$, $55\% \pm 5\%$ humidity, and a 12-hour day-night cycle (lighting time: 8:30 am).

Ethics statement

All experimental methods were performed in accordance with the regulations and procedures of the Institutional Animal Care and Use Committee (approval number: JBNU 021-0184) of Jeonbuk National University and followed the 3R principles of replacement, reduction, and refinement (24).

SH101 Roborovski hamster experiments

The COVID-19 infection animal model was created by directly injecting 50 μ L of SARS-CoV-2 suspension [10⁵ x 50% tissue culture infectious dose (TCID)₅₀] into the nasal cavity of hamsters. The dosages and conditions for P108 and vehicle substances for each group are described in Table 1. The sample for the efficacy test of P108 was formulated based on a 20 g hamster weight, using sterile distilled water for the dilution. P108 was formulated at concentrations of 1,000 mg/kg/10 mL and 3,000 mg/kg/10 mL using sterile distilled water for injection for administration to animals. The dosage of P108

was determined with reference to the daily intake (2.7 g/day/person) approved by the Korean Ministry of Food and Drug Safety for PF501, an anti-obesity health functional food derived from Korean perilla leaves using a comparable extraction method (25). Based on a standard human body weight of 60 kg, this corresponds to approximately 45 mg/ kg/day. Using body surface area normalization (Km factor: human = 37; hamster = 5), the equivalent dose for hamsters was calculated to be approximately 333 mg/kg/day. For efficacy evaluation, P108 was administered at two dose levels: 1000 mg/kg and 3000 mg/kg, representing approximately 3-fold and 9-fold multiples of the human-equivalent dose, respectively. The test substance for administration was prepared as follows; After 15 min of vortexing, P108 solution was sonicated in a 40 °C water bath for another 15 min, followed by five more minutes of vortexing. The test material was prepared on the day of administration and vortexed for an additional 5 min immediately before administration. For the positive control group, Paxlovid (20 mg/kg/day) was prepared by dissolving the active components in a small volume of dimethyl sulfoxide (DMSO), followed by dilution with sterile distilled water to achieve a final DMSO concentration of 0.5% (v/v). The solution was vortexed for 15 min, sonicated in a 40 °C water bath for 15 min, and vortexed again for 5 min. After filtration through a 0.2 µm syringe filter, the solution was aliquoted and stored at -20°C. Prior to administration, it was vortexed again for 5 min and administered orally.

All experimental groups, infection status, oral dosing regimens, and vehicle compositions are summarized in Table 1, including the Paxlovid formulation and final DMSO concentration. Unless otherwise specified, primary comparisons were made against the vehicle (saline) control group.

A total of 50 female Roborovski hamsters, aged 3 months, were divided into five groups: normal control (mock-infected, saline PO),

TABLE 1 Summary of the experimental groups.

Group	Sex	Number of animals		Virus infection	Article	Sample administration period and virus infection timing
Normal Control (0 mg/kg)	Female	5 (sacrified at 5 dpi)	5 (sacrified at 10 dpi)	DMEM 50 μL / head	-	Oral administration of samples for 9 Days post-infection (dpi) Starting from 0 dpi
Vehicle (saline) control	Female	5 (sacrified at 5 dpi)	5 (sacrified at 10 dpi)		Saline, 200 μL / head	
Low P108 (1000 mg/kg)	Female	5 (sacrified at 5 dpi)	5 (sacrified at 10 dpi)	SARS-CoV-2	Low concentration of Korean perilla leaf ethanol extract P108, 200 µL / head	
High P108 (3000 mg/kg)	Female	5 (sacrified at 5 dpi)	5 (sacrified at 10 dpi)	(10 ⁵ TCID ₅₀) 50 μL / head	High concentration of Korean perilla leaf ethanol extract P108, 200 μL / head	
Positive (paxlovid) Control (20 mg/kg)	Female	5 (sacrified at 5 dpi)	5 (sacrified at 10 dpi)		Paxlovid, 200 μL / head	

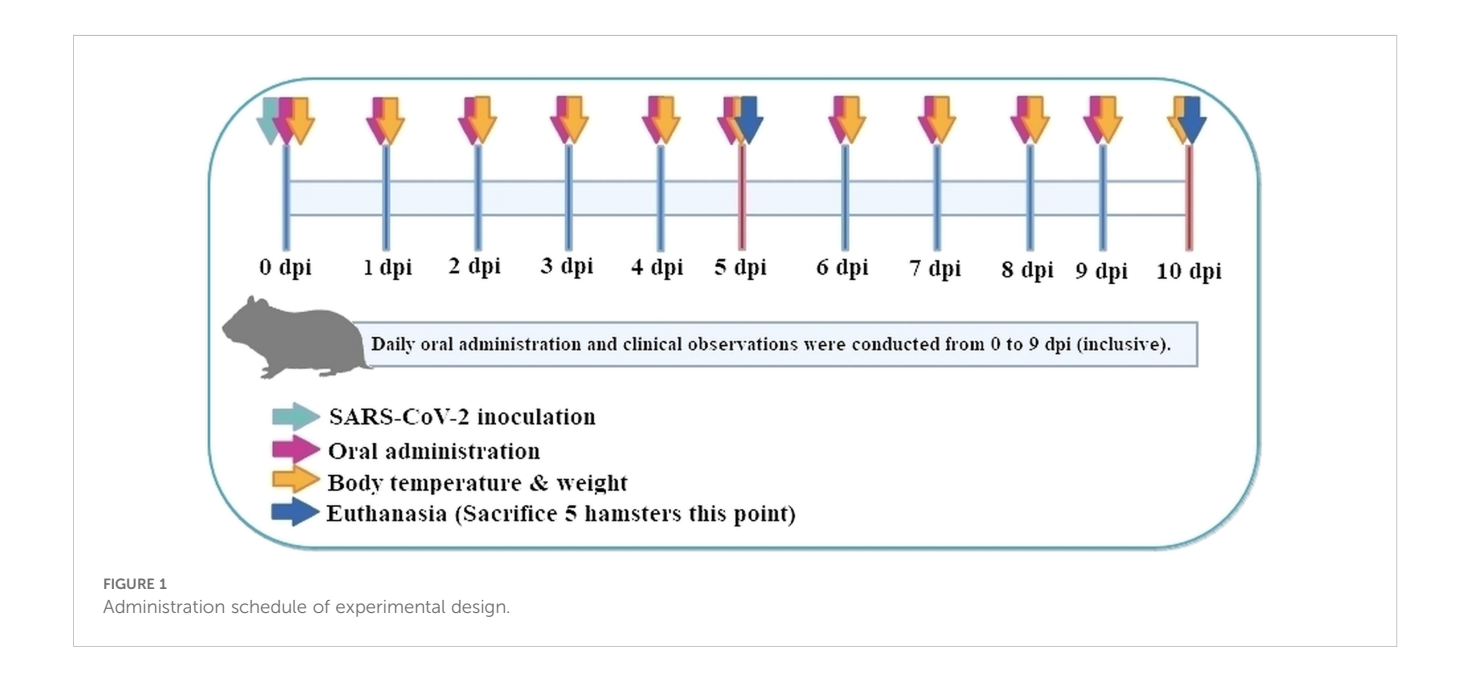
vehicle control (SARS-CoV-2-infected, saline), low-dose and highdose P108, and a positive control (Paxlovid formulated in DMSO + water). Full dosing details and vehicle compositions are provided in Table 1, and each group consisted of 10 hamsters. Healthy animals selected during the acclimatization period were weighed. Then those animals with body weight closest to the mean were selected and distributed randomly as shown in the 'group identification' table so each group had a comparable weight distribution. The groups were labeled as normal control, vehicle control, low P108, high P108, and positive control (A control group receiving only the excipients used for Paxlovid administration was not included in the study design). As shown in Figure 1, the experiment was conducted over 10 days. At 0 days post-inoculation (dpi), all groups except the normal control group were intranasally inoculated with 50 µL of SARS-CoV-2 suspension (10⁵ x TCID₅₀). At day 5 dpi, five animals from each group were euthanized for analysis, and the remaining animals were euthanized at 10 dpi. On the scheduled necropsy day, euthanasia was performed for each group under deep isoflurane anesthesia (3-5% inhaled). After blood sampling, the animals were sacrificed by exsanguination by transecting the posterior vena cava and abdominal aorta. The normal control group received 50 µL of Dulbecco's modified Eagle medium (DMEM; Thermo Fisher Scientific, Waltham, MA, USA) in place of SARS-CoV-2 suspension, and 100 µL of saline was administered orally. The vehicle control group received 50 µL of SARS-CoV-2 suspension (10⁵ TCID₅₀) in the nasal cavity to induce COVID-19 infection, followed by 200 µL/head of saline administered orally. For the pharmacological evaluation of P108, animals were restrained by gently securing the dorsal skin, and 200 µL of P108 suspension was orally administered into the stomach using a sonde attached to a syringe. In the positive control group, 50 µL of SARS-CoV-2 suspension (10⁵ TCID₅₀) was intranasally inoculated, followed by oral administration of 200 µL of Paxlovid suspension per animal.

Cell cultures and viral infections

The SARS-CoV-2 strain used for COVID-19 infection was obtained from the National Culture Collection for Pathogens (NCCP) of the Korea Disease Control and Prevention Agency. Full genome information for this SARS-CoV-2 strain is available at Global Initiative on Sharing All Influenza Data (identifier: BetaCoV/Wuhan/ IVDC-HB-01/2020 EPI_ISL_402119), and the strain is also registered with the China Microbial Data Center (accession number NMDC10013001; genome accession number MDC60013002-01). The SARS-CoV-2 strain was propagated by infecting Vero cells in DMEM supplemented with 10% fetal bovine serum (FBS), 100 IU/ml penicillin, and 100 ug/ml streptomycin, and incubated at 37 °C and 5% CO₂, atomosphere. After four to seven days of incubation the cells were examined microscopically for cytopathic effects. When more than 50% of the cells exhibited cytopathic changes, the culture supernatant was harvested and centrifuged at 450xg for 5 minutes to remove cell debris. The clarified supernatant was aliquoted into 200 ul vials and used for experiments.

Clinical observation

Changes in hamster body temperature due to SARS-CoV-2 virus infection and drug administration were measured using a thermal imaging camera (Teledyne FLIR LLC, Wilsonville, OR, USA), and the thermal images were analyzed as body temperature using the DirA program (Teledyne FLIR). The highest temperature point in the chest closest to the lungs was considered the body temperature of each hamster. Changes in hamster body weight due to SARS-CoV-2 virus infection and drug administration were measured using a scale, and the percent weight change was calculated as (current weight/0 dpi weight) × 100%.



D-dimer and fibrin degradation product analyses

The blood analysis of the hamsters was performed as follows. First, whole blood was collected from the hamsters in each group through cardiac puncture at 5 dpi and 10 dpi. The collected blood was centrifuged for 10 min at 2,500 \times g. The serum fraction was carefully harvested and immediately frozen at -80°C for later analysis. Serum D-dimer and FDP levels were analyzed using quantitative enzyme-linked immunosorbent assay (ELISA) kits: the hamster D-dimer (D2D) ELISA kit (MBS012417; MyBioSource Inc., San Diego, CA, USA) and the hamster FDP ELISA kit (MBS005821; MyBioSource Inc.). Samples for quantitative analysis were prepared by diluting them 10 times with a sample diluent solution: 50 µL of each diluted sample was dropped into the wells of a micro-ELISA plate coated with antibodies against D-dimer or FDP, and then reacted at 37°C for 60 min, followed by 15 min of reaction with a chromogen solution, before stopping the reaction with a stop solution. Immediately after stopping the reaction, the optical density at 450 nm (OD 450) was measured with an ELISA reader (i Mark Microplate Absorbance Reader, Bio-Rad Laboratories, Inc., Hercules, CA, USA). From at least two measurements, the average OD 450 was calculated, and the blank OD 450 was subtracted to obtain the final mean OD 450 of each sample. The concentrations of D-dimer and FDP were calculated from the OD 450 values obtained from each sample using a standard curve.

Interleukin-6, tumor necrosis factor- α , and IL-10 analyses

Quantitative analyses of IL-6, TNF-α, and IL-10 in hamster serum were carried out using a hamster IL-6 ELISA kit (MBS7606648; MyBioSource, Inc.), hamster TNF-α ELISA kit (MBS7606475; MyBioSource, Inc.), and hamster IL-10 ELISA kit (MBS8819724; MyBioSource, Inc.), respectively, using regular ELISA methods. Serum samples for cytokine analysis and corresponding standards were prepared by 10-fold dilution in sample diluent. Standards were further prepared by serial dilution in the same buffer. A 100 µL aliquot of each diluted sample or standard was added to micro-ELISA wells pre-coated with capture antibodies for IL-6, TNF-α, or IL-10 and incubated at 37°C for 90 min. Plates were washed, incubated with horseradish peroxidase-streptavidin, washed again, and developed with chromogenic substrate according to the manufacturer's instructions. The reaction was stopped, and absorbance at 450 nm (OD450) was measured using a microplate reader (iMark Microplate Absorbance Reader, Bio-Rad, Hercules, CA, USA). Measurements were performed in duplicate; mean OD450 values were blank-corrected. Cytokine concentrations were calculated from 4-parameter logistic standard curves with the following ranges: IL-6, 7.8-500 pg/mL; TNF-\alpha, 3.125-200 pg/mL; IL-10, 6.25-400 pg/mL.

Quantitative analysis of SARS-CoV-2

Virologic quantitation in hamster lungs in the vehicle, positive, and P108 groups was carried out as follows. The SH101 Roborovski hamsters belonging to the vehicle, positive, and P108 groups were euthanized at 5 dpi and 10 dpi, then dissected and lung organs were separated. A portion of the separated left lung lobe was homogenized using a tissue homogenizer, followed by centrifugation at 3,000 rpm for 10 min at 4°C. The supernatant obtained was treated with a RNeasy® Mini kit (QIAGEN; Hilden, Germany) to extract the RNA and prepare the sample according to the manual. A reverse transcription-quantitative polymerase chain reaction (RT-qPCR) was then performed with a PrimerScript RT Reagent kit (Takara Holdings Inc., Kyoto, Japan). The primers used were the forward primer: 5'-GCCTCTTCTCGTTCCTCATCAC-3' and the reverse primer: 5'-AGCAGCATCACCGCCATTG-3', targeting the envelope gene of the SARS-CoV-2 virus. The RTqPCR reaction was carried out under the following conditions using an iQTM SYBR[®] Green Supermix kit (Bio-Rad Laboratories Inc.): DNA Denaturation, 95°C for 3 min; and DNA amplification, 40 cycles (15 sec at 95 °C, 30 sec at 60 °C). The real-time polymerase chain reaction standard curve was generated by serial dilution of the recombinant plasmid and was used as a quantitation standard. The cycle threshold values for each sample were used to quantify the viral titer using the standard curve.

Lung pathology

Following euthanasia, the chest cavity of each hamster was opened, and the lungs were dissected. The entire lungs were photographed using a digital camera. Then, the lung tissues were immediately fixed in 10% neutral buffered formalin solution to facilitate staining with hematoxylin and eosin (H&E) as previously described (26). Changes in lung tissue, such as infiltration of inflammatory cells and thickening of the interstitial tissue, were observed under an optical microscope.

Analysis of immune cells in blood using flow cytometry

Hamster blood was collected at 5 dpi and 10 dpi, and Peripheral blood mononuclear cells (PBMCs) were stained with Alexa Fluor700 anti-CD3e, APC anti-CD4, FITC anti-CD8a, and PE anti-CD16 antibodies, and incubated at 4°C for 20 min. Flow cytometry analysis was performed using a FACSymphony TM A3 system, with results analyzed using FlowJo TM version 10.8.1 software (Becton Dickinson). Due to the study's focus on CD8+, CD3+/CD28+, CD8+/CD28+, and CD16+ cell populations, CD4+ T cell data were not analyzed. Flow cytometry data were analyzed following a predefined gating strategy: FSC/SSC leukocyte gate → singlets (FSC-H vs. FSC-A) → live cells (viability dye negative) → CD3+ T cells → CD4+ and CD8a+ subsets; NK cells were identified

as CD3⁻CD16⁺. Compensation was performed using single–stained controls, and positive gates were defined using FMO controls. Gating was performed in the following sequential order: (1) leukocytes were identified by forward scatter (FSC) versus side scatter (SSC); (2) singlets were selected using FSC–H versus FSC–A to exclude doublets and aggregates; (3) live cells were gated as viability dye–negative (viability dye: Zombie Aqua, dilution 1:100); (4) CD3⁺ T cells were defined by Alexa Fluor 700 signal, and CD4⁺ and CD8⁺ subsets were identified within the CD3⁺ gate using APC and FITC signals, respectively; (5) monocytes were defined as CD14 (PE–Cy7) positive, and CD16 (PE) positive cells were identified as NK/other CD16⁺ populations.

A minimum of 100,000 lymphocyte—gate events were acquired per sample. Compensation matrices were generated using Thermo Fisher OneComp single—color compensation beads (or equivalent single—color beads). Positive/negative thresholds were set based on fluorescence minus one (FMO) controls.

Statistical analysis

All quantitative data, excluding histopathological findings that were qualitatively assessed based on incidence, were presented as mean ± standard deviation (SD), and statistical analyses were performed using SPSS Statistics 12.0K (for Medical Science). To confirm SARS-CoV-2 infection, comparisons were made between the normal control and vehicle (saline) control groups. Treatment effects were evaluated by comparing the test groups (low and high P108) with the vehicle control group, unless otherwise specified. Given that Paxlovid was formulated in a DMSO/water mixture, a DMSO-only vehicle control group was not included. To validate the

experimental system, comparisons between the vehicle control and positive control groups were conducted using Student's t-test. For multiple group comparisons, one-way ANOVA was followed by Duncan's or Dunnett's post hoc test, depending on the experimental context. Where multiple pairwise comparisons were performed, Bonferroni correction was applied to adjust for type I error. Body temperature, body weight, serum levels, SARS-CoV-2 mRNA expression levels, and flow cytometry results were analyzed using above method. Histopathological incidence was assessed using the nonparametric Mann-Whitney U test. All statistical tests were two-sided, and no formal power calculations were conducted. Statistical significance was defined as p < 0.05 or p < 0.01.

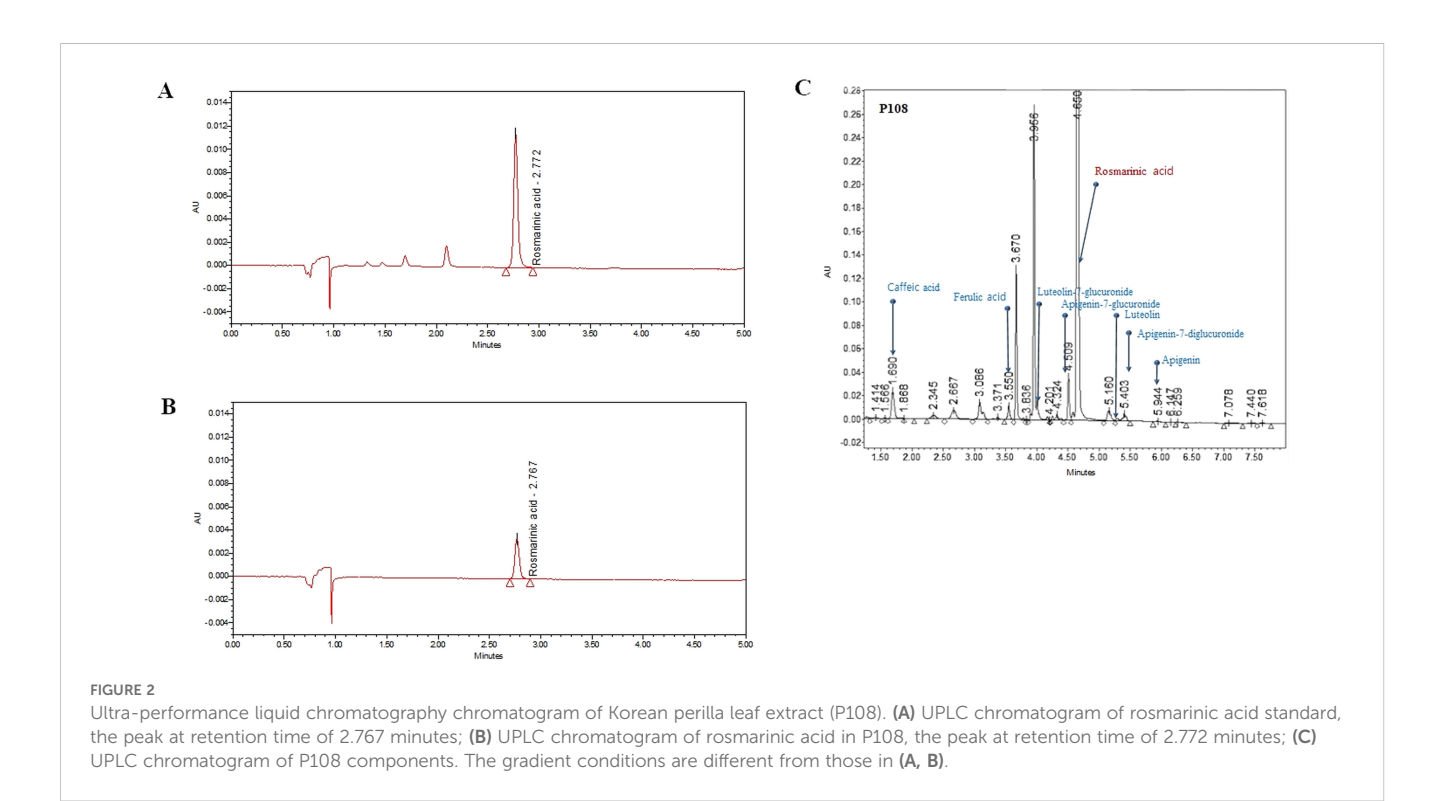
Results

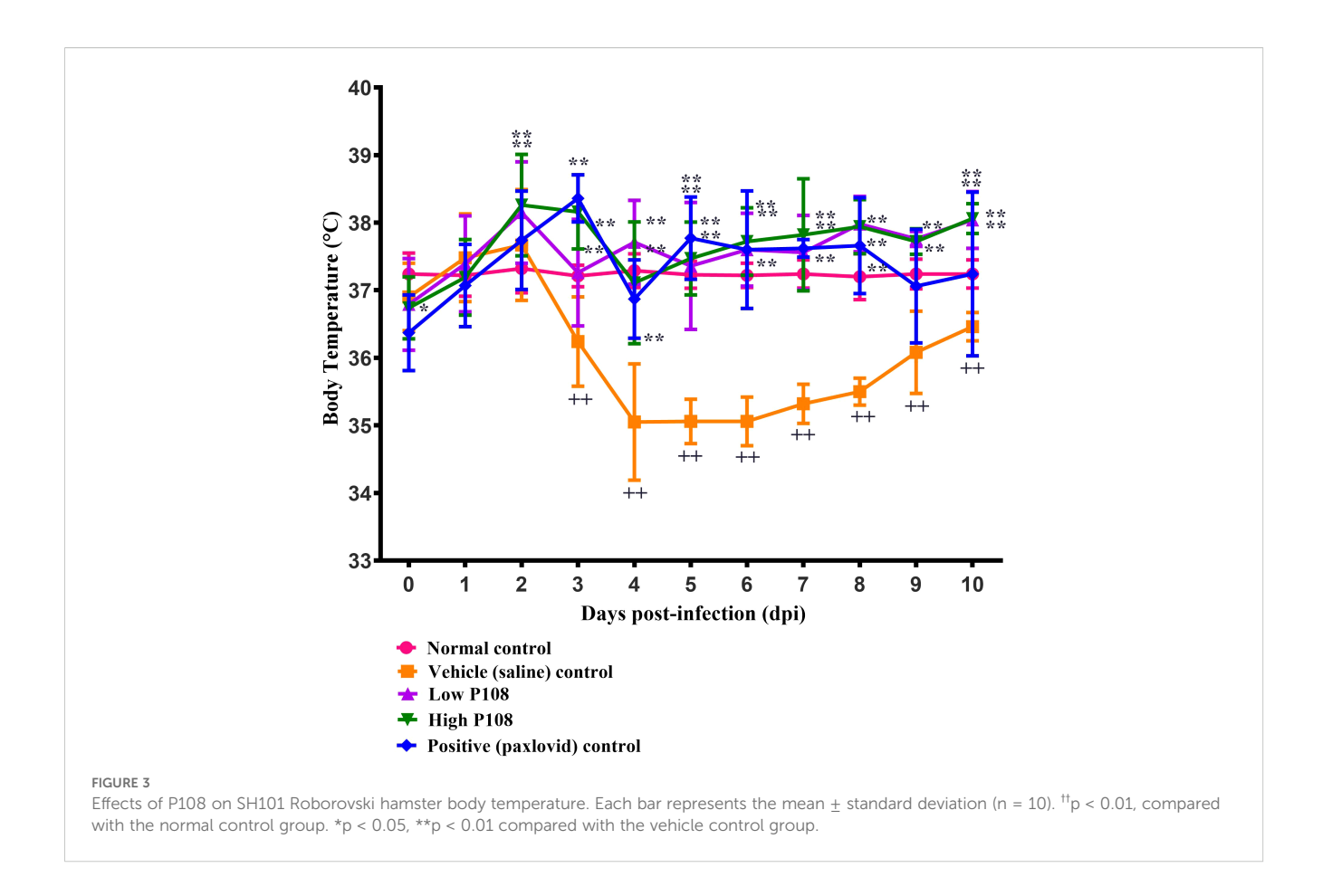
UPLC analysis

As shown in Figure 2, the average concentration of the marker compound, rosmarinic acid in P108 was 115.2 μ g/mg. In addition to rosmarinic acid, 0.6% caffeic acid, 0.09% luteolin, and several trace constituents were detected.

Effects of P108 on body temperature and weight

The vehicle control group showed a gradual decrease in body temperature from 3 dpi, indicating hypothermia (Figure 3). In contrast, the low and high P108 groups and the positive control group exhibited a slight fever at 2–3 dpi, followed by a return to





temperatures similar to the normal control group. After SARS-CoV-2 infection, the high P108 group and the positive control group initially showed a slight decrease in body weight, but by 8 dpi, the body weights recovered to levels comparable to those of the normal control group (Figure 4). In contrast, the low P108 group showed greater weight loss than the high P108 group and failed to recover to the levels of the normal control group.

Effects of P108 on blood clot formation

Figure 5 shows the levels of D-dimer and FDP in the blood measured in each group of hamsters. The vehicle control group had an increase in D-dimer (Figure 5A) and FDP (Figure 5B) levels compared to the normal control group. At 5 dpi, there was no decrease in clotting due to the administration of P108 or paxlovid, but at 10 dpi, the FDP levels were significantly reduced in both the low and high P108 groups compared to the vehicle control group (p < 0.05).

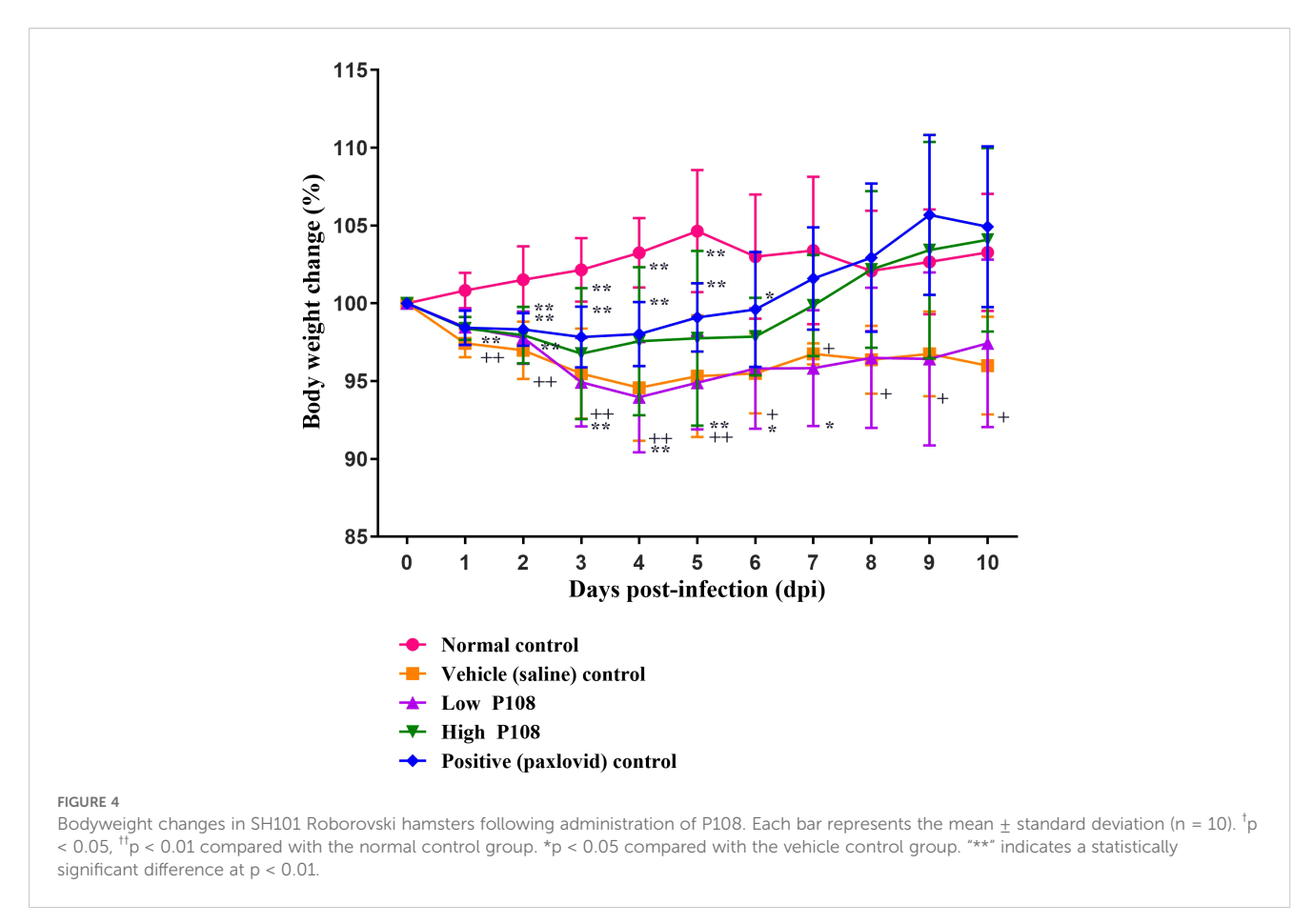
Effects of P108 on cytokine levels

At 5 dpi, serum IL-6 levels were significantly reduced by 28% and 32% in the low and high P108 groups, respectively (p < 0.05), compared to the vehicle control group. At 10 dpi, reductions of 26%

and 38% were observed in the respective groups (p < 0.01) (Figure 6A). TNF-α levels increased by 19% in the vehicle control group at 5 dpi due to viral infection (p < 0.01), but were significantly decreased by 36% and 24% in the low and high P108 groups, respectively (p < 0.01). The positive control group also showed a 32% reduction (p < 0.01). At 10 dpi, although no statistically significant differences were observed, TNF-α levels increased by 18% in the vehicle control group and decreased by 15% and 17% in the low and high P108 groups, respectively (Figure 6B). At 5 dpi, serum IL-10 levels were significantly elevated by 69% and 77% in the low and high P108 groups, respectively (p < 0.05), compared to the vehicle control group. At 10 dpi, increases of 64% (p < 0.01) and 54% (p < 0.05) were observed in the respective groups (Figure 6C). Although the positive control group also showed an increase in IL-10 levels, the difference was not statistically significant relative to the vehicle control group.

Effects of P108 on right lung histopathology

The results of lung histopathological examination are summarized in Table 2. Figures 7A, B show the normal control group with minimal inflammatory changes and well-organized lung architecture. In contrast, Figures 7C, D depict the vehicle control



group, where the lungs display pronounced inflammation characterized by red spots, increased size and number of lesions, and a disorganized cellular arrangement with a significant presence of inflammatory cells. Figures 7E, F represent the low P108 group, where inflammation is still evident but appears to be somewhat alleviated compared to the vehicle control. Figures 7G-J show the high P108 and positive control groups, which showed a marked reduction in inflammation, indicating a more organized lung structure and fewer inflammatory cells. Overall, the P108 groups exhibit milder lung inflammation compared to the vehicle control group. Additionally, the severity of inflammation was greater at 5 dpi than at 10 dpi, highlighting the potential therapeutic effects of P108 over time.

Effects of P108 on SARS-CoV-2 replication

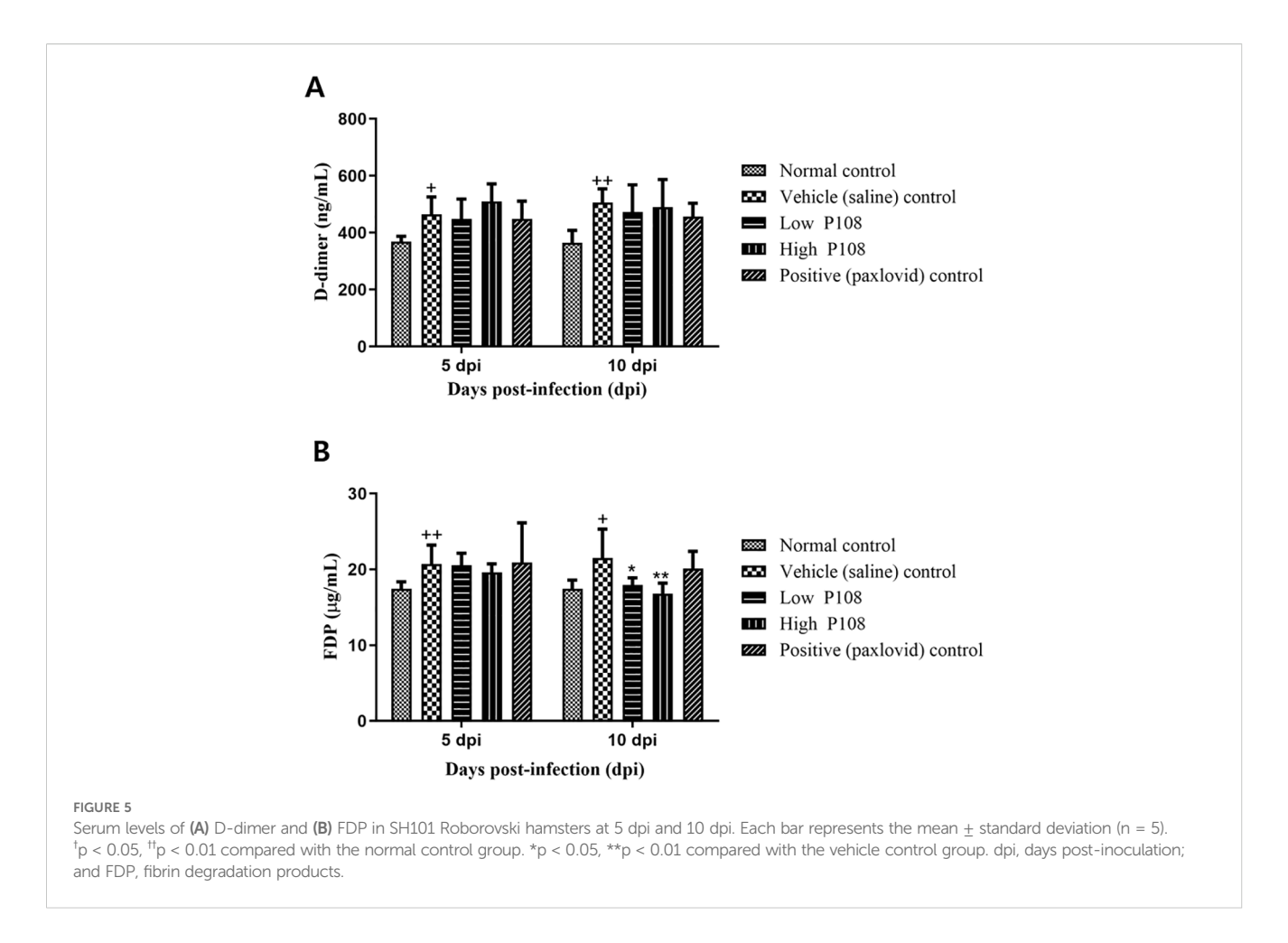
In the vehicle control group, $1.14\times10^4\pm2.22\times10^3$ mRNA copies/g tissue was detected at 5 dpi and $6.99\times10^3\pm2.49\times10^3$ mRNA copies/g tissue was detected at 10 dpi (Figure 8). In contrast, significantly lower viral loads were observed in the P108 groups and the positive control group. Notably, at 5 dpi, the high P108 group and the positive control group showed reductions of 27% (p < 0.05) and 30% (p < 0.05), respectively, compared to the vehicle control group. However, at 10 dpi, the virus reduction rates in the P108 groups were not significantly different from those in the vehicle control group.

Effects of P108 on host immune readouts: cytokines and T/NK-cell subsets

Immune cells such as CD8 $^+$ T cells and CD16 $^+$ NK cells suppress viral activity through direct and indirect mechanisms. To evaluate immune cell dynamics following SARS-CoV-2 infection, blood samples collected at 5 and 10 dpi were analyzed by flow cytometry. At 5 dpi, the low P108 group showed significant increases in CD8 $^+$, CD3 $^+$ /CD28 $^+$, and CD8 $^+$ /CD28 $^+$ T cell populations compared to the vehicle control group (Figures 9A–C; p < 0.05). At 10 dpi in the low-dose group, as well as at 5 and 10 dpi in the positive control and high-dose P108 groups, the observed levels of the previously mentioned T-cell subsets (CD8 $^+$, CD3 $^+$ /CD28 $^+$, CD8 $^+$ /CD28 $^+$) showed mild increases compared to the vehicle control group without statistical significance. No significant differences in CD16 $^+$ NK cells were noted at 10 dpi. CD4 $^+$ T cells were not included in the analysis, as the study focused on CD8 $^+$, CD3 $^+$ /CD28 $^+$, CD8 $^+$ /CD28 $^+$, and CD16 $^+$ subsets to assess the immunomodulatory effects of P108.

Discussion

SARS-CoV-2 is a virus that caused a cluster outbreak of pneumonia in December 2019 in Wuhan, China. Since its emergence in Wuhan, SARS-CoV-2 has persisted from March 2020 to May 2023, infecting over 689 million people and causing 6.9 million deaths globally (27). Vaccines against COVID-19

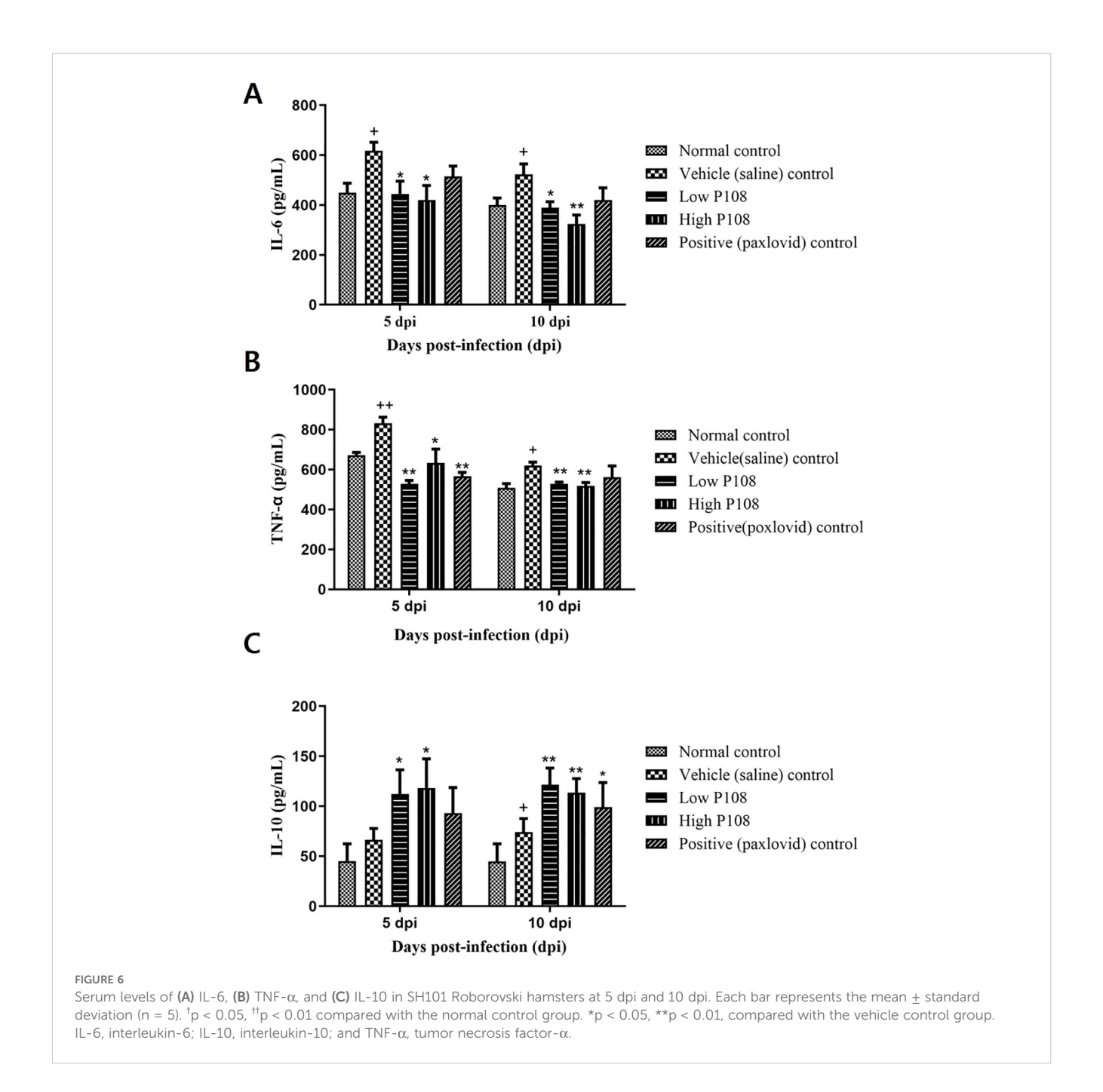


infection were developed in 2021; however, despite the completion of booster shots in many countries worldwide, the virus is persisting, forming new variants, and continuing to infect people (3, 4). All viruses, including COVID-19, can evolve and can result in the emergence of different strains. Many widely used modern pharmaceuticals and vaccines have been praised for their rapid and potent efficacy, but long-term use can lead to drug resistance and various side effects (28). Some natural products have been utilized as pharmaceuticals, and the development of drugs derived from edible plants may offer a solution to this dilemma, owing to their relatively low toxicity and diverse bioactivities, including antiviral properties (29, 30). For example, Chinese perilla leaf water extract reportedly inhibited SARS-CoV-2 replication in cell lines and Syrian hamster models (23, 31, 32). This study aimed to evaluate the therapeutic potential of Korean perilla leaf extract (P-108) against SARS-CoV-2 infection. To this end, experiments were conducted using SH101 Roborovski hamsters, a model known to exhibit COVID-19-like symptoms that closely resemble those observed in humans (13). While the SH101 hamster provides a rigorous platform for assessing candidate interventions, extrapolation to humans should be approached with caution due to model-specific limitations and the small sample sizes employed in this study.

In a recent study, a notable pattern of initial weight loss followed by a subsequent recovery in body mass was observed in Syrian hamsters infected with COVID-19 (33). In the present study, the high P108 group, and the positive control group, showed a relatively low rate of body weight change. As weight loss is a prominent characteristic of severe COVID-19, the low rate of bodyweight change in this study suggests that hamsters administered a high P108 dose remained in a mild symptomatic state, even when infected with SARS-CoV-2, and avoided progression to severe COVID-19.

The occurrence of hypothermia after fever is a typical progression pattern in severe COVID-19 and is observed in humans and animal models (13, 34). Hypothermia is presumed to result from severe infection, leading to marked reduction in physical activity and decreased energy metabolism. In this study, the high P108 group and the positive control group exhibited a slight fever at 3 to 4 dpi and then returned to normal body temperature, similar to the normal control group. Therefore, in both the high P108 group and the positive control group, some prevention of SARS-CoV-2 infection from progressing to severe COVID-19 infection may have occurred.

Blood clot formation is another key feature of COVID-19, particularly severe COVID-19, and blood levels of D-dimer and FDP are key indicators of thrombus formation (35, 36). Inflammatory changes activate fibrogenesis, resulting in elevated D-dimer and FDP levels, and there is ample evidence linking inflammatory activation and thrombosis during severe infections.



Hyper-inflammatory conditions also induce endothelial damage and D-dimer levels are associated with an increased risk of venous thromboembolism in patients with COVID-19 (37–39). In this study, the vehicle control group had increased D-dimer and FDP levels compared to the normal control group. Meanwhile, in the low and high P108 groups, the levels of FDP were significantly decreased at 10 dpi, suggesting that clot formation was inhibited by P108 administration.

Blood concentrations of pro-inflammatory cytokines are important indicators of the degree of inflammation that occurs in the body when bacteria or viruses invade and cause infection (40, 41). The serious consequences of COVID-19 are associated with respiratory failure and cytokine release syndrome, with the rise of IL-6 as a predictive parameter. Therefore, IL-6 is a promising

therapeutic target for anti-cytokine treatment in severe cases of COVID-19 (42). TNF- α -mediated inflammation can also cause harmful tissue damage and gradually promote pulmonary fibrosis, leading to subsequent pneumonia, pulmonary edema, and acute respiratory distress syndrome in patients with COVID-19 infection (43). In this study, the significant decreases in IL-6 and TNF- α observed in the low and high P108 groups indicate that P108 inhibits IL-6 and TNF- α ; both of these cytokines can induce inflammation in the body during SARS-CoV-2 virus infection (44).

Unlike the pro-inflammatory cytokines IL-6 and TNF- α , the anti-inflammatory cytokine IL-10 plays a crucial role in suppressing inflammatory responses (44). IL-10 helps regulate excessive inflammation during viral infections and maintains immune system balance (45, 46). Thus, IL-10 levels increase during viral

TABLE 2 Effects of P108 on right lung histopathology in SH101 Roborovski hamsters infected with SARS-CoV-2.

Findings	Groups								
	Normal control	Vehicle (saline) control	Low P108	High P108	Positive (paxlovid) control				
Interstitial inflammation									
5 dpi - ^{a)}	4	0	0	0	0				
+	1	0	2	1	1				
++	0	2	2	4*	4*				
+++	0	3	1	0	0				
10 dpi -	4	0	0	0	0				
+	1	2	1	4	3				
++	0	2	4	1	2				
+++	0	1	0	0	0				
Peribronchiolar inflammation									
5 dpi -	5	1	0	0	1				
+	0	0	3	5	3				
++	0	4	2	0	1				
+++	0	0	0	0	0				
10 dpi -	5	2	0	3	2				
+	0	2	3	2	2				
++	0	1	2	0	1				
+++	0	0	0	0	0				

Data are presented as number of animals.

a) Grades are as follows: -; Normal (Lung tissue appears histologically normal); +; Slight (Minimal inflammatory cell infiltration and slight thickening of the interstitial tissue. Changes are subtle and localized); ++; Moderate (Noticeable infiltration of inflammatory cells and moderate interstitial thickening. Alterations are more widespread than slight); +++; Marked (Prominent inflammatory cell infiltration and considerable interstitial thickening. Structural changes are evident and extensive but not severe).

*p < 0.05 compared with the vehicle control group.

infections and IL-10 may protect against inflammation. The significant increases in serum IL-10 levels observed in the low and high P108 groups in this study show that oral administration of perilla leaf extract suppresses the inflammatory response after SARS-CoV-2 infection.

CD4+ T cells are known to play a critical role in antiviral immune responses by recognizing pathogens and coordinating immune cell activity (46). In this study, CD4+ T cells were not analyzed due to the focus on CD8⁺, CD3⁺/CD28⁺, CD8⁺/CD28⁺, and CD16⁺ populations. Future studies investigating CD4+ T cell responses could further elucidate P108's immunomodulatory effects. CD8+ cells, also known as cytotoxic T cells, function by directly destroying infected cells used for viral replication (47). Therefore, CD4⁺ and CD8⁺ cells suppress the virus through direct and indirect interactions. In the present study, the significant increases in CD8+ cells in the low dose P108 group and increase trend of high dose P108 group and positive control group after viral infection demonstrate the potential efficacy of P108 in treating COVID-19. Notably, although the low-dose P108 group showed significant reductions in IL-6 and TNF- α and elevations in IL-10 (Figure 6), together with the most pronounced increase in CD8⁺ and CD28⁺ T cells (Figure 9), these animals nonetheless experienced persistent weight loss without signs of recovery (Figure 4). Moreover, lung viral RNA levels in the low-dose group were not significantly reduced compared to the vehicle control at 10 dpi (Figure 8). The reduction in pulmonary viral RNA with high-dose P108 suggests potential effects on early viral processes (e.g., entry or replication) or augmentation of host antiviral responses. Plant-derived constituents in Perilla frutescens have been reported to influence host pathways that can restrict viral propagation. In our model, the timing of viral load reduction at 5 dpi is consistent with an effect on acute replication kinetics and/or antiviral signaling, which warrants targeted mechanistic studies. This discrepancy suggests that while low-dose P108 is sufficient to trigger immunomodulatory changes and enhance cellular immune responses, the antiviral effect at this dose may not reach the threshold required for effective viral clearance and systemic recovery. In contrast, the high-dose P108 group achieved both immunomodulation and significant viral load reduction, which correlated with restored body weight and improved clinical outcomes. These findings support the notion that adequate viral suppression, in addition to immune modulation, is necessary to achieve full therapeutic benefit in this model.

 $\mbox{CD28}^{+}$ T cells support the survival and function of activated T cells during viral infections, and T cells effectively participate in attacking and destroying infected cells (48, 49). In this study, $\mbox{CD3}^{+}/$ $\mbox{CD28}^{+}$ T-cell levels showed a significant decrease in the vehicle

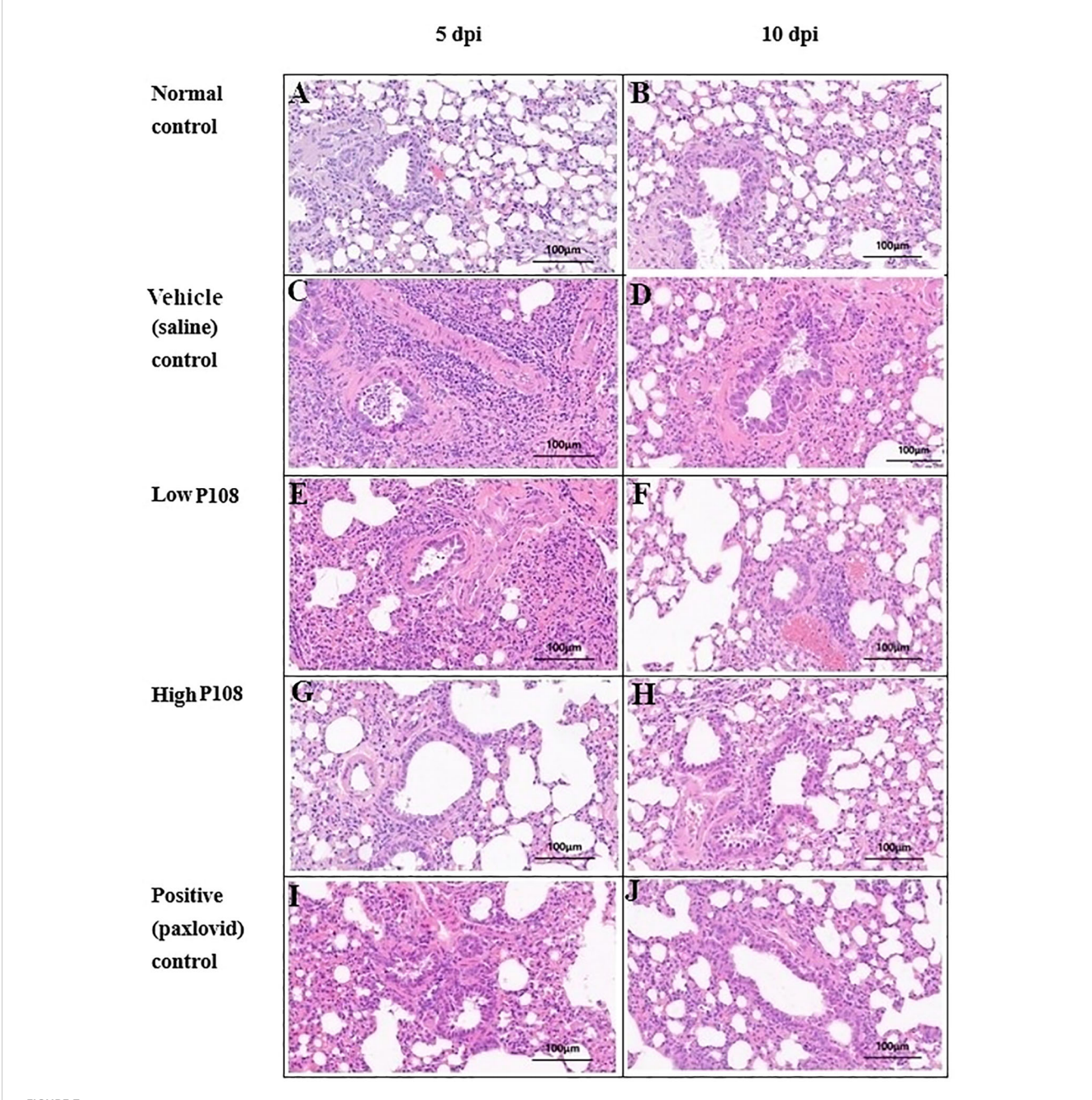
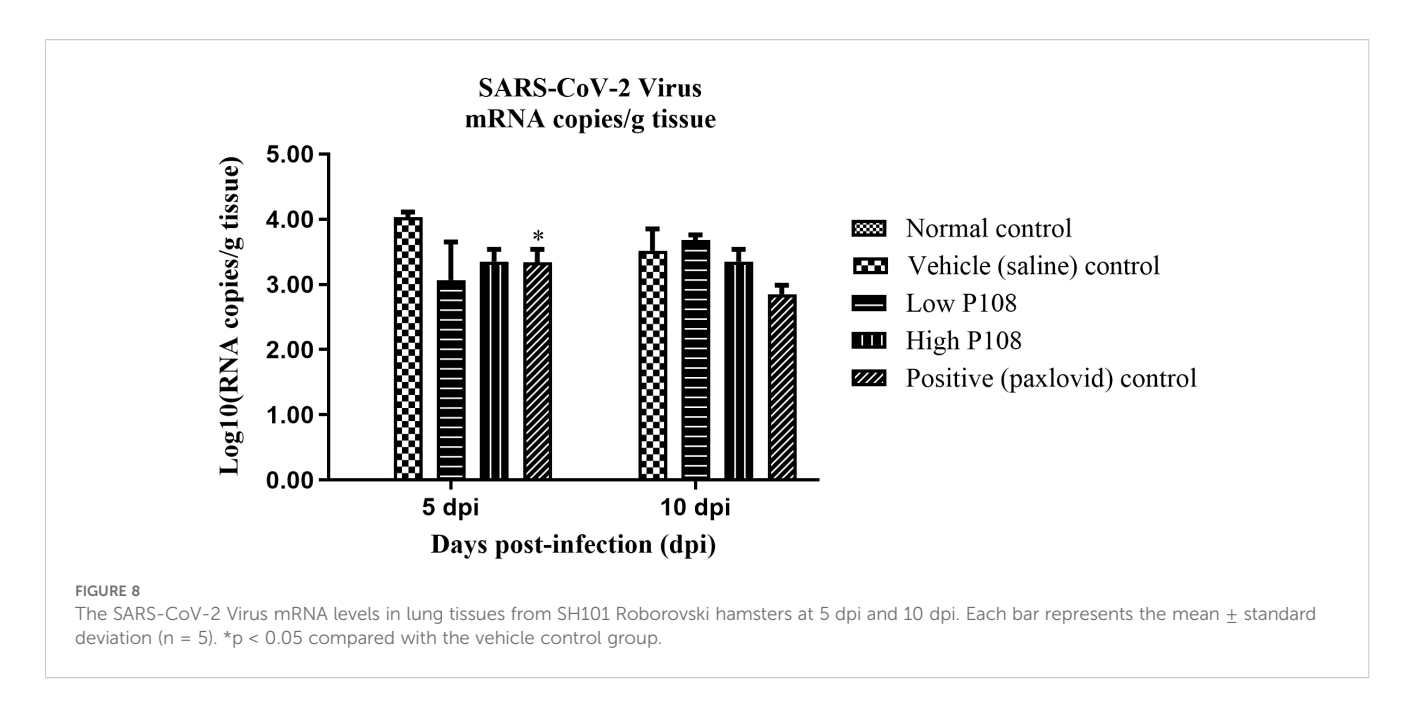


FIGURE 7
Histologic assessment (H&E staining) of right lung tissues collected from SH101 Roborovski hamsters at 5 dpi and 10 dpi. (A, B) Normal control; (C, D) Vehicle (saline) control; (E, F) Low P108; (G, H) High P108; (I, J) Positive (paxlovid) control. The right lung tissues in the vehicle control group showed increased inflammatory cells centered around the alveoli, whereas the P108 groups showed a general decrease in inflammatory cells. dpi, days post-inoculation; H&E, hematoxylin and eosin.

control group following viral infection. In contrast, a significant increase was observed in the low-dose P108 group at 5 dpi, while upward trends without statistical significance were noted at 10 dpi in the low-dose group, as well as at both 5 and 10 dpi in the high-dose P108 and positive control groups. These indicate that P108 has a positive effect on CD28⁺ T-cell expression, and suggests a potential therapeutic role for P108 in modulating T-cell responses that are important for viral defense mechanisms.

The interaction of CD8⁺ and CD28⁺ T cells is essential for regulating the activation and function of CD8⁺ cells (50). Although clear dose–response relationships were not established, immune cell changes—including CD8⁺/CD28⁺ and CD16⁺ T-cell subsets—showed similar patterns in both P108-treated groups and the positive control group (51). These findings suggest that P108 may have potential as a COVID-19 therapeutic by modulating immune responses associated with viral clearance (52).

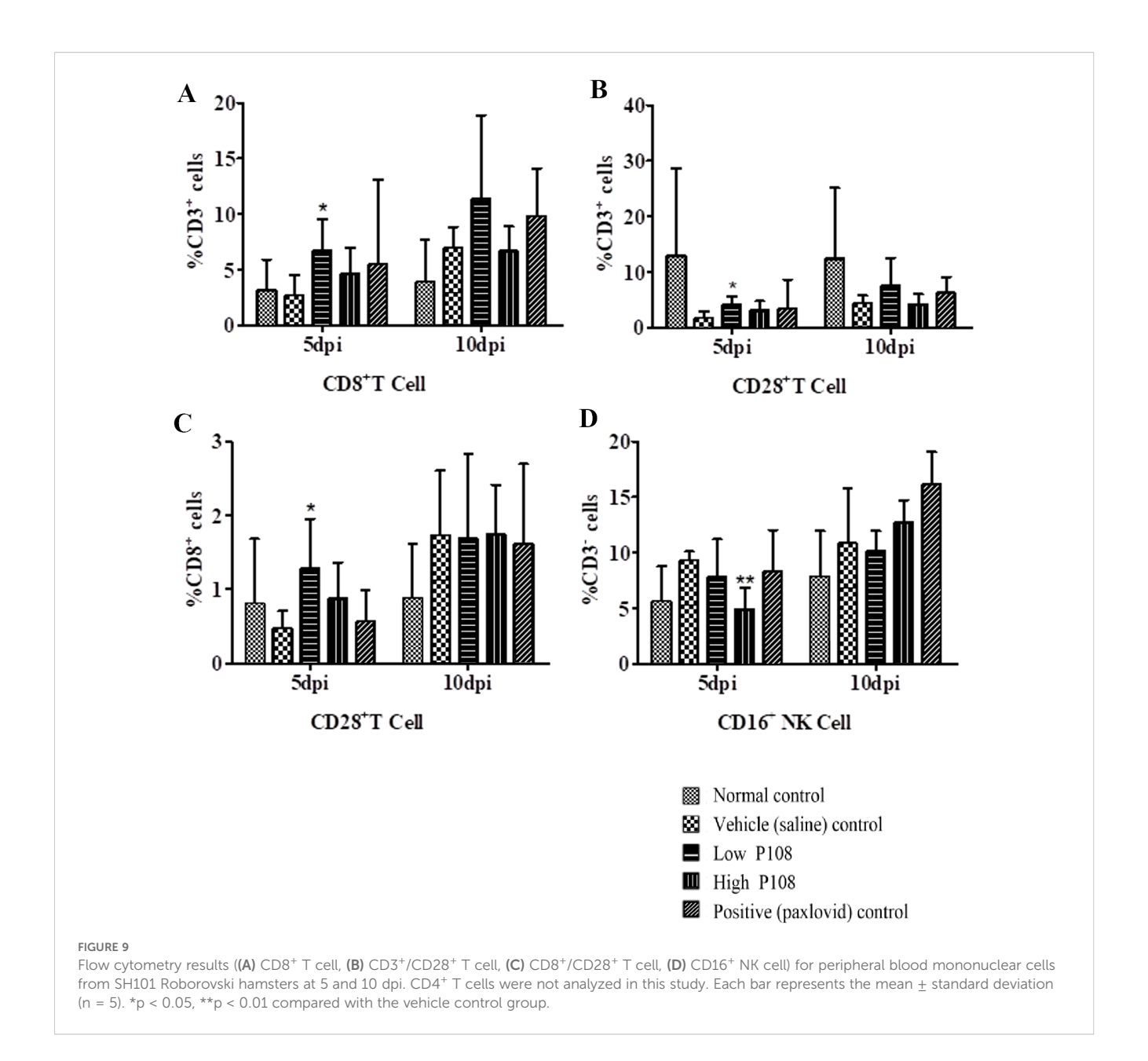


Histologic examination of right lung tissue plays a critical role in the diagnosis and understanding of various respiratory diseases, especially infections, inflammatory responses, cancer, and other lung diseases (53). Such examination can observe microstructural changes in lung tissue and help to reveal the pathologic mechanisms of diseases and determine appropriate treatment strategies (52). In the present study, histopathologic examination of right lung tissue stained with H&E revealed that hamsters in the low and high P108 groups (compared to the vehicle control group) had significantly fewer inflammatory cells (e.g., macrophages, neutrophils widely distributed throughout the alveoli and interstitial tissues) in the lungs, a finding associated with alleviation of lung inflammation. These histopathological changes were comparable to those observed in the Paxlovid-treated group, suggesting that P-108 may also exert therapeutic effects at the tissue level.

The dose-dependent reduction in viral load observed in the lungs of the high P108 group confirms that SARS-CoV-2 replication was inhibited by P108 administration. Rosmarinic acid and caffeic acid, the main marker compounds in Korean perilla leaves, have antiinflammatory, antioxidant, antiviral, and antibacterial effects (19, 53). In this study, the administered amounts of rosmarinic acid in the P108 treatment groups at doses of 1000 mg/kg/day and 3000 mg/kg/ day were calculated to be 115 mg/kg/day and 345 mg/kg/day, respectively. These values were derived based on the rosmarinic acid content of P108, which was determined to be 115.2 µg/mg. Recent In silico studies have identified rosmarinic acid as a promising multi-targeted inhibitor against SARS-CoV-2. Its antiviral activity is attributed to interactions with both viral and host proteins critical for viral entry and replication. Specifically, rosmarinic acid exhibits binding affinity to ACE2 (Angiotensin-Converting Enzyme 2), the primary receptor for viral entry, potentially preventing viral attachment to host cells. It also interferes with TMPRSS2 (Transmembrane Serine Protease 2), a host serine protease responsible for spike protein priming, thereby disrupting membrane fusion. Furthermore, rosmarinic acid targets key viral enzymes such as 3CLpro (3C-like protease) and PLpro (Papain-Like Protease), which are essential for processing viral polyproteins, leading to inhibition of viral replication. Its molecular flexibility and ability to form non-covalent interactions—including hydrogen bonding and dipole stabilization—enable effective engagement with multiple viral targets, supporting its potential as a broad-spectrum antiviral agent (54, 55). Although the oral bioavailability of rosmarinic acid has been reported to be relatively low in rodent models (approximately 0.91-1.69%), its pharmacological activity in vivo remains evident (56). While specific bioavailability data in hamsters are not currently available, the therapeutic effects observed in this study suggest that rosmarinic acid, a major constituent of P-108, may exert meaningful biological effects despite limited systemic exposure. These findings support the continued investigation of P-108 and its active components in the context of COVID-19 intervention strategies. In contrast, the concentrations of caffeic acid and luteolin analyzed in P108 were found to be very low. Therefore, we consider it unlikely that these compounds contributed significantly to the observed antiviral effects.

The results of this study suggest that P108 administration may suppress SARS-CoV-2 replication in both experimental animals and humans.

Although the number of hamsters tested at 5 and 10 days post-infection (dpi) was limited (n = 5 per group), the observed changes support the potential of P108 as a prophylactic or early-intervention therapeutic agent, particularly under a post-exposure prophylaxis-like design. It should be noted, however, that this study was not designed to evaluate the efficacy of P108 in treating advanced stages of COVID-19. The small sample size increases the risk of Type I and Type II errors, especially in the context of multiple comparisons involving cytokines (IL-6, TNF- α , IL-10) and flow cytometry subsets (CD8+, CD3+/CD28+, CD8+/CD28+, CD16+). Furthermore, statistical power calculations were not performed due to the preliminary nature of the study, which may have limited the ability to detect subtle therapeutic effects.



To mitigate these constrains, future studies will incorporate larger sample sizes and formal power analyses to enhance statistical rigor and reduce error risks. Encouragingly, therapeutic effects observed across multiple parameters in the positive control group validate the experimental design and reinforce the reliability of the study methodology. Moreover, the high-dose P108 treatment group exhibited changes comparable to those of the positive control group across most evaluation metrics.

Despite the limitations, the consistent therapeutic responses observed in the high-dose P108 group indicate promising potential for P108 as a candidate for COVID-19 treatment. These preliminary results warrant further investigation through well-powered and rigorously designed studies to confirm its efficacy and support future clinical development.

Previous studies have reported that water extracts of Chinese perilla leaves inhibit RNA and protein synthesis of SARS-CoV-2, significantly reducing virus-induced cytokine release as well as viral protein and RNA levels (23). Taken together, although the botanical sources differ at the species level and extraction method, the results from this study, along with previous reports on Chinese perilla leaf extracts, may collectively support the potential of perilla-derived substances as promising candidates for COVID-19 therapy.

Meanwhile, the potential toxicity of P-108 used in this study is considered to be very low, given that Korean perilla leaves have long been consumed as a safe dietary component in Korea. Furthermore, as previously mentioned, PF501—an ethanol extract derived from Korean perilla leaves and structurally similar to P-108—has been officially approved as a functional health food in Korea, further

supporting the safety profile of P-108 (25). Although the test substance used in that study differs from P-108, a previous subchronic toxicity study demonstrated that repeated oral administration of perilla seed oil—extracted from Korean perilla seeds—for 90 days in beagle dogs did not result in any adverse effects at doses up to 3,000 mg/kg/day. This finding provides additional supportive evidence regarding the safety of perilladerived compounds (57, 58).

In summary, this study offers preliminary evidence for the potential efficacy of P-108. However, further research—including GLP-compliant toxicology, identification of active or marker compounds, and clinical evaluation—is needed before advancing P-108 as a botanical drug candidate. Although the Paxlovid formulation contained a low concentration of DMSO (0.5% v/v), a DMSO-only vehicle control was not included, leaving room for possible vehicle-related effects. No apparent DMSO-associated changes were observed, but future studies will incorporate a matched vehicle control to improve data interpretation.

Conclusion

In a post-exposure prophylaxis-like model using SH101 Roborovski hamsters, once-daily oral administration of P-108 for 10 days effectively reduced SARS-CoV-2 replication and mitigated inflammation, likely through modulation of host immune responses. The dose used (1,000 mg/kg/day) corresponds to approximately 135 mg/kg/day in humans, equivalent to 15.6 mg/ kg/day of rosmarinic acid. These findings support further investigation of P-108 as a potential prophylactic or earlyintervention agent against COVID-19. However, its efficacy under delayed treatment conditions, such as administration after symptom onset, remains to be determined. Future studies should incorporate larger sample sizes with sufficient statistical power, explore potential synergy with approved COVID-19 therapeutics, and conduct mechanistic analyses to elucidate immune-modulatory and antiviral pathways. Notably, the therapeutic potential of P-108 may be further enhanced by leveraging its existing formulation as a 500 mg tablet, which has already been approved as a health functional food for anti-obesity purposes using a similar extract (25).

Significance statement

This study demonstrates that oral administration of Korean perilla leaf ethanol extract (P-108) exhibits therapeutic potential in the SH101 Roborovski hamster model of SARS-CoV-2 infection, as evidenced by reductions in viral RNA levels, attenuation of inflammatory responses, and histopathological improvements. These preclinical results support the continued evaluation of P-108 as a candidate for prophylactic or early-intervention strategies against COVID-19. However, further validation through larger-scale and clinically oriented studies is warranted to confirm its efficacy and safety in human populations.

Data availability statement

The original contributions presented in the study are included in the article/supplementary material. Further inquiries can be directed to the corresponding authors.

Ethics statement

The animal study was approved by Institutional Animal Care and Use Committee (approval number: JBNU 021-0184) of Jeonbuk National University and followed the 3R principles of replacement, reduction, and refinement. The study was conducted in accordance with the local legislation and institutional requirements.

Author contributions

J-SA: Data curation, Formal Analysis, Visualization, Writing – original draft, Writing – review & editing. W-IK: Software, Validation, Visualization, Writing – review & editing. S-TH: Conceptualization, Investigation, Supervision, Writing – review & editing. H-MK: Data curation, Investigation, Methodology, Writing – original draft. O-YK: Formal Analysis, Investigation, Methodology, Writing – review & editing. J-HL: Investigation, Methodology, Visualization, Writing – review & editing. YK: Supervision, Validation, Writing – review & editing. S-WS: Conceptualization, Funding acquisition, Project administration, Supervision, Writing – review & editing. J-CK: Supervision, Validation, Writing – review & editing, Writing – original draft. M-HL: Formal Analysis, Investigation, Methodology, Software, Writing – review & editing.

Funding

The author(s) declare that no financial support was received for the research and/or publication of this article.

Conflict of interest

Authors J-SA, OY-K, JH-L, YK, M-HL, and S-WS were employed by the company CorestemChemon Inc.

The remaining authors declare that the research was conducted in the absence of any commercial or financial relationships that could be construed as a potential conflict of interest.

Generative AI statement

The author(s) declare that no Generative AI was used in the creation of this manuscript.

Any alternative text (alt text) provided alongside figures in this article has been generated by Frontiers with the support of artificial

intelligence and reasonable efforts have been made to ensure accuracy, including review by the authors wherever possible. If you identify any issues, please contact us. reviewers. Any product that may be evaluated in this article, or claim that may be made by its manufacturer, is not guaranteed or endorsed by the publisher.

Publisher's note

All claims expressed in this article are solely those of the authors and do not necessarily represent those of their affiliated organizations, or those of the publisher, the editors and the

Supplementary material

The Supplementary Material for this article can be found online at: https://www.frontiersin.org/articles/10.3389/fviro.2025. 1685444/full#supplementary-material

References

- 1. Qin E, Zhu Q, Yu M, Fan B, Chang G, Si B, et al. A complete sequence and comparative analysis of a SARS-associated virus (Isolate BJ01). *Chin Sci Bull.* (2003) 48:941–8. doi: 10.1007/BF03184203
- 2. Muralidar S, Ambi SV, Sekaran S and Krishnan UM. The emergence of COVID-19 as a global pandemic: understanding the epidemiology, immune response and potential therapeutic targets of SARS-CoV-2. *Biochimie*. (2020) 179:85–100. doi: 10.1016/j.biochi.2020.09.018
- 3. Meo SA, Bukhari IA, Akram J, Meo AS, Klonoff DC. COVID-19 vaccines: comparison of biological, pharmacological characteristics and adverse effects of Pfizer/BioNTech and moderna vaccines. *Eur Rev Med Pharmacol Sci.* (2021) 25:1663–9. doi: 10.26355/eurrev_202102_24877
- 4. Chenchula S, Karunakaran P, Sharma S, Chavan M. Current evidence on efficacy of COVID-19 booster dose vaccination against the Omicron variant: a systematic review. *J Med Virol.* (2022) 94:2969–76. doi: 10.1002/jmv.27697
- Ita K. Coronavirus disease (COVID-19): Current status and prospects for drug and vaccine development. Arch Med Res. (2021) 52:15–24. doi: 10.1016/j.arcmed.2020.09.010
- 6. Hassan W, Kazmi SK, Tahir MJ, Ullah I, Royan HA, Fahriani M Global acceptance and hesitancy of COVID-19 vaccination: A narrative review. *Narra J.* (2021) 1:e57. 1–12. doi: 10.52225/narra.v1i3.57
- 7. Zheng J, Wong LYR, Li K, Verma AK, Ortiz ME, Wohlford-Lenane C, et al. COVID-19 treatments and pathogenesis including anosmia in K18-hACE2 mice. *Nature*. (2021) 589:603–7. doi: 10.1038/s41586-020-2943-z
- 8. de Farias LPG, Fonseca EKUN, Strabelli DG, Loureiro BMC, Neves YCS, Rodrigues TP, et al. Imaging findings in COVID-19 pneumonia. *Clinics*. (2020) 75: e2027. doi: 10.6061/clinics/2020/e2027
- 9. Fa Z, Chen L, Li J, Cheng X, Yang J, Tian C, et al. Clinical features of COVID-19-related liver functional abnormality. *Clin Gastroenterol Hepatol.* (2020) 18:1561–6. doi: 10.1016/j.cgh.2020.04.002
- 10. Cleary SJ, Pitchford SC, Amison RT, Carrington R, Robaina Cabrera CL, Magnen M, et al. Animal models of mechanisms of SARS-CoV-2 infection and COVID-19 pathology. *Brit J Pharmacol.* (2020) 177:4851–65. doi: 10.1111/bph.15143
- 11. Kevadiya BD, Machhi J, Herskovitz J, Oleynikov MD, Blomberg WR, Bajwa N, et al. Diagnostics for SARS-coV-2 infections. *Nat Mater.* (2021) 20:593–605. doi: 10.1038/s41563-020-00906-z
- 12. Chan JFW, Zhang AJ, Yuan S, Poon VKM, Chan CCS, Lee ACY, et al. Simulation of the clinical and pathological manifestations of coronavirus disease 2019 (COVID-19) in a golden Syrian hamster model: implications for disease pathogenesis and transmissibility. *Clin Infect Dis.* (2020) 71:2428–46. doi: 10.1093/cid/cia/325
- 13. Zhai C, Wang M, Chung HJ, Hassan M, Lee S, Kim HJ, et al. Roborovski hamster (Phodopus roborovskii) strain SH101 as a systemic infection model of SARS-CoV-2. *Virulence.* (2021) 12:2430–42. doi: 10.1080/21505594.2021.1972201
- 14. Lim SU, Seo YH, Lee YG, Baek NI. Isolation of volatile allelochemicals from leaves of *Perilla frutescens* and Artemisia asiatica. *Appl Biol Chemist*. (1994) 37:115–23.
- 15. Cho BO, Yin HH, Fang CZ, Ha HO, Kim SJ, Jeong SI, et al. Synergistic anti-inflammatory effect of rosmarinic acid and luteolin in lipopolysaccharide-stimulated RAW264.7 macrophage cells. *Korean J Food Sci Technol.* (2015) 47:119–25. doi: 10.9721/KJFST.2015.47.1.119
- 16. Ahmed HM. Ethnomedicinal, phytochemical and pharmacological investigations of Perilla frutescens (L.) Britt. *Molecules*. (2018) 24:102. doi: 10.3390/molecules24010102
- 17. Lim H, Shin S. Anti-Bacillus and anti-Shigella activities of the essential oil from Perilla fruescens var. japonica Hara. J Essent Oil Bear Pl. (2014) 17:309–16. doi: 10.1080/0972060X.2014.895157
- 18. Kim DJ, Assefa ADA, Jeong YJ, Jeon YA, Lee JE, Lee MC, et al. Variation in fatty acid composition, caffeic and rosmarinic acid content, and antioxidant activity of

perilla accessions. Korean J Med Crop Sci. (2019) 27:96–107. doi: 10.7783/KJMCS.2019.27.2.96

- 19. Chircov C, Pîrvulescu DC, Bîrcă AC, Andronescu E, Grumezescu AM. Magnetite microspheres for the controlled release of rosmarinic acid. *Pharmaceutics*. (2022) 14:2292. doi: 10.3390/pharmaceutics14112292
- 20. Pavlíková N. Caffeic acid and diseases mechanisms of action. *Int J Mol Sci.* (2022) 24:588
- 21. Jeong JH, Park HJ, Chi GY, Choi YH, Park SH. An ethanol extract of *Perilla frutescens* leaves suppresses adrenergic agonist-induced metastatic ability of cancer cells by inhibiting src-mediated EMT. *Molecules*. (2023) 28:3414. doi: 10.3390/molecules28083414
- 22. Bassoli A, Borgonovo G, Caimi S, Scaglioni L, Morini G, Schiano Moriello A, et al. Taste-guided identification of high potency TRPA1 agonists from Perilla frutescens. *Bioorg Med Chem.* (2009) 17:1636–9. doi: 10.1016/j.bmc.2008.12.057
- 23. Tang WF, Tsai HP, Chang YH, Chang TY, Hsieh CF, Lin CY, et al. Perilla (Perilla frutescens) leaf extract inhibits SARS-CoV-2 via direct virus inactivation. Biomed J. (2021) 44:293–303. doi: 10.1016/j.bj.2021.01.005
- 24. Lee KH, Lee DW, Kang BC. The 'R' principles in laboratory animal experiments. *Lab Anim Res.* (2020) 36:45. doi: 10.1186/s42826-020-00078-6
- $25. \ Available \ online \ at: \ https://data.mfds.go.kr/hid/opbab01/prdtDtlInfo.do \ (Accessed January 12, 2025).$
- 26. Seo HS, Kim JH, Kim SH, Park MK, Seong NW, Kang GH, et al. Toxicity of a 90-day repeated oral dose of a collagen peptide derived from skate (*Raja kenojei*) skin: a rat model study. *Toxicol Res.* (2023) 39:383–98. doi: 10.1007/s43188-023-00175-3
- 27. Stróż S, Kosiorek P, Stasiak-Barmuta A. The COVID-19 inflammation and high mortality mechanism trigger. Immunogenetics.~(2024)~76:15–25. doi: 10.1007/s00251-023-01326-4
- 28. Yuan H, Ma Q, Ye L, Piao G. The traditional medicine and modern medicine from natural products. *Molecules*. (2016) 21:559. doi: 10.3390/molecules21050559
- 29. Antonio ADS, Wiedemann LSM, Veiga-Junior VF. Natural products' role against COVID-19. RSC Adv. (2020) 10:23379–93. doi: 10.1039/D0RA03774E
- 30. Tassakka ACMAR, Iskandar IW, Juniyazaki ABA, Zaenab S, Alam JF, Rasyid H, et al. Green algae Caulerpa racemosa compounds as antiviral candidates for SARS-CoV-2: In silico study. *Narra J.* (2023) 3:e79. 1–11. doi: 10.52225/narra.v3i2.179
- 31. Chin YF, Tang WF, Chang YH, Chang TY, Lin WC, Lin CY, et al. Orally delivered perilla (Perilla frutescens) leaf extracteffectively inhibits SARS-CoV-2 infection in a Syrian hamster model. *J Food Drug Anal.* (2022) 30:252–70. doi: 10.38212/2224-6614.3412
- 32. Jan JT, Cheng TJ R, Juang YP, Ma HH, Wu YT, Yang WB, et al. Identification of existing harmaceuticals and herbal medicines as inhibitors of SARS-CoV-2 infection. *Proc Natl Acad Sci U.S.A.* (2021) 118:1–8. doi: 10.1073/pnas.2021579118
- 33. Imai M, Iwatsuki-Horimoto K, Hatta M, Loeber S, Halfmann PJ, Nakajima N, et al. Syrian hamsters as a small animal model for SARS-CoV-2 infection and countermeasure development. *Proc Natl Acad Sci USA*. (2020) 117:16587–95. doi: 10.1073/pnas.2009799117
- 34. Fan C, Wu Y, Rui X, Yang Y, Ling C, Liu S, et al. Animal models for COVID-19: advances, gaps and perspectives. *Signal Transduction Targeting Ther.* (2022) 7:220. doi: 10.1038/s41392-022-01087-8
- 35. Koo HL, Kwon HJ, Lee WT. Pathological features of COVID-19 pneumonia diagnosed following an autopsy. *Korean J Leg Med.* (2021) 45:145–9. doi: 10.7580/kjlm.2021.45.4.145
- 36. Moresco RN, Júnior RH, Cláudio RVL, Mariano DRSL. Association between plasma levels of D-dimer and fibrinogen/fibrin degradation products (FDP) for exclusion of thromboembolic disorders. *J Thromb Thrombolysis*. (2006) 21:199–202. doi: 10.1007/s11239-006-4837-9
- 37. Srivastava S, Garg I, Bansal A, Kumar B. COVID-19 infection and thrombosis. Clin Chim Acta. (2020) 510:344–6. doi: 10.1016/j.cca.2020.07.046

- 38. Levi M, Keller TT, Gorp EV, Cate HT. Infection and inflammation and the coagulation system. *Cardiovasc Res.* (2003) 60:26-39. doi: 10.1016/S0008-6363(02) 00857-X
- 39. Pizzi R, Gini G, Caiano L, Castelli B, Dotan N, Magni F, et al. Coagulation parameters and venous thromboembolism in patients with and without COVID-19 admitted to the emergency department for acute respiratory insufficiency. *Thromb Res.* (2020) 196:209–12. doi: 10.1016/j.thromres.2020.09.004
- 40. Watkins LR, Maier SF, Goehler LE. Immune activation: the role of proinflammatory cytokines in inflammation, illness responses and pathological pain states. *Pain*. (1995) 63:289–302. doi: 10.1016/0304-3959(95)00186-7
- 41. Upadhyay J, Tiwari NN, Ansari MN. Role of inflammatory markers in corona virus disease (COVID-19) patients: a review. *Exp Biol Med.* (2020) 245:1368–75. doi: 10.1177/1535370220939477
- 42. Gubernatorova EO, Gorshkova EA, Polinova AI, Drutskaya MS. IL-6: relevance for immunopathology of SARS-CoV-2. *Cytokine Growth Factor Rev.* (2020) 53:13–24. doi: 10.1016/j.cytogfr.2020.05.009
- 43. Mohd Zawawi Z, Kalyanasundram J, Mohd Zain R, Thayan R, Basri DF, Yap WB. Prospective roles of tumor necrosis factor-alpha (TNF- α) in COVID-19: prognosis, therapeutic and management. *Int J Mol Sci.* (2023) 24:6142. doi: 10.3390/ijms24076142
- 44. Han H, Ma Q, Li C, Liu R, Zhao L, Wang W, et al. Profiling serum cytokines in COVID-19 patients reveals IL-6 and IL-10 are disease severity predictors. *Emerg Microbes Infect.* (2020) 9:1123–30. doi: 10.1080/22221751.2020.1770129
- 45. Vries JE. Immunosuppressive and anti-inflammatory properties of interleukin 10. *Ann Med.* (1995) 27:537–41. doi: 10.3109/07853899509002465
- 46. Toes RE, Ossendorp F, Offringa R, Melief CJ. CD4 T cells and their role in antitumor immune responses. *J Exp Med.* (1999) 189:753–6. doi: 10.1084/jem.189.5.753
- 47. Wong P, Pamer EG. CD8 T cell responses to infectious pathogens. Ann Rev Immunol. (2003) 21:29–70. doi: 10.1146/annurev.immunol.21.120601.141114
- 48. Hunt PW, Martin JN, Sinclair E, Bredt B, Hagos E, Lampiris H, et al. T cell activation is associated with lower CD4+ T cell gains in human immunodeficiency

virus-infected patients with sustained viral suppression during antiretroviral therapy. *J Infect Dis.* (2003) 9:1123–30. doi: 10.1086/374786

- 49. Linterman MA, Denton AE, Divekar DP, Zvetkova I, Kane L, Ferreira C, et al. CD28 expression is required after T cell priming for helper T cell responses and protective immunity to infection. *Elife*. (2014) 3:e03180. doi: 10.7554/eLife.03180.016
- 50. Strioga M, Pasukoniene V, Characiejus D. CD8+ CD28– and CD8+ CD57+ T cells and their role in health and disease. Immunology. (2011) 134:17–32. doi: 10.1111/j.1365-2567.2011.03470.x
- 51. Cooper MA, Fehniger TA, Caligiuri MA. The biology of human natural killer-cell subsets. *Trends Immunol.* (2001) 22:633–40. doi: 10.1016/S1471-4906(01)02060-9
- 52. Pedersen BK, Hoffman-Goetz L. Exercise and the immune system: regulation, integration, and adaptation. *Physiol Rev.* (2000) 80:1055–81. doi: 10.1152/physrev.2000.80.3.1055
- 53. Seo YS, Park KH, Park JM, Jeong H, Kim B, Jeon JS, et al. Short-term inhalation exposure to cigarette smoke induces oxidative stress and inflammation in lungs without systemic oxidative stress in mice. *Toxicol Res.* (2024) 40:273–83. doi: 10.1007/s43188-023-00223-v
- 54. Kumar S, Kumar V. Rosmarinic acid as a potential multi-targeted inhibitor for SAR-coV-2: an in silico virtual screening approach. *Coronaviruses.* (2024) 5: e181223224611. 11–20. doi: 10.2174/0126667975275509231211062032
- 55. Patel U, Desai K, Dabhi RC, Maru JJ, Shrivastav PS. Bioprospecting phytochemicals of Rosmarinus officinalis L. for targeting SARS–CoV–2 main protease (Mpro): a computational study: An In silico Virtual Screening Approach. *J Mol Modeling.* (2023) 29:161. doi: 10.1007/s00894-023-05569-6
- 56. Wang JX, Li GY, Rui TQ, Kang A, Li GC, Fu TM, et al. Pharmacokinetics of rosmarinic acid in rats by LCMS/MS: absolute bioavailability and dose proportionality. *RSC Adv.* (2017) 7:9057–63. doi: 10.1039/C6RA28237G
- 57. Pannone G, Caponio VCA, De Stefano IS, Ramunno MA, Meccariello M, Agostinone A, et al. Lung histopathological findings in COVID-19 disease–a systematic review. *Infect Agent Cancer.* (2021) 16:34. doi: 10.1186/s13027-021-00369-0
- 58. Zhang HX, Guan J, Tian YH, Su GY, Zhao YQ. Acute and sub-chronic 90-day oral toxicity study of Perilla seed oil in rodents and Beagle dogs. *Regul Toxicol Pharmacol.* (2019) 103:229–36. doi: 10.1016/j.yrtph.2019.01.035